Journal of Alloys and Compounds 509 (2011) 9351–9355

Contents lists available at ScienceDirect

Journal of Alloys and Compounds

journal homepage: www.elsevier.com/locate/jallcom

Electrophoretic enhanced micro arc oxidation of ZrO_2–HAp–TiO_2 nanostructured porous layers

F. Samanipour[a], M.R. Bayati[a,b,*], H.R. Zargar[c], F. Golestani-Fard[a,d], T. Troczynski[c], M. Taheri[a]

[a] School of Metallurgy and Materials Engineering, Iran University of Science and Technology, P.O. Box 16845-161, Tehran, Iran
[b] Department of Materials Science and Engineering, North Carolina State University, Raleigh, NC, USA
[c] Department of Metals and Materials Engineering, University of British Columbia, Vancouver, BC V6T 1Z4, Canada
[d] Center of Excellence for Advanced Materials, Iran University of Science and Technology, P.O. Box 16845-195, Tehran, Iran

ARTICLE INFO

Article history:
Received 9 May 2011
Received in revised form 11 July 2011
Accepted 13 July 2011
Available online 23 July 2011

Keywords:
Micro arc oxidation
Electrophoretic deposition
Composite
Coating
Porous

ABSTRACT

Micro arc oxidation (MAO) and electrophoretic deposition (EPD) processes were simultaneously employed to grow ZrO_2–HAp–TiO_2 porous layers on titanium substrates under different conditions. Influence of the electrolyte composition and the growth time on surface morphology, topography, phase structure, and stoichiometry of the layers was investigated. The utilized electrolytes consisted of β-glycerophosphate, calcium acetate, sodium phosphate, and micron sized yttria-stabilized zirconia with different concentrations. AFM and SEM evaluations revealed a rough surface with a porous structure with a pores size of 50–750 nm. The pores size increased with the time and the electrolyte concentration. Based on the XRD and XPS results, the layers consisted of anatase, hydroxyapatite, monoclinic ZrO_2, tetragonal ZrO_2, ZrO, $CaTiO_3$, and α-TCP phases whose fractions were observed to change depending on the synthesis conditions. The average crystalline size of the HAp phase was determined as ~54 nm. The nano-sized zirconia particles (d = 20–60 nm) were dispersed not only on surface, but also in depth of the layers. Utilizing thicker electrolytes and prolonging the growth time resulted in decomposition of hydroxyapatite as well as tetragonal ZrO_2 to monoclinic ZrO_2. EDX results also showed that the zirconium wt% in the layers increased with the time. EPD-enhanced MAO (EEMAO) technique was expressed as an efficient route to fabricate ZrO_2–HAp–TiO_2 multiphase systems within short times and only in one step.

1. Introduction

In recent years, much attentions have been directed to hydroxyapatite (HAp, $Ca_{10}(PO_4)_6(OH)_2$) as a substitute material for damaged teeth or bones due to its similarities with mineral component of hard tissues of vertebrates [1–3]. Its bioactivity results in proliferation of osteoblasts to HAp [4,5]. Unfortunately, this biomaterial has poor mechanical properties and, hence, is not suitable for load-bearing conditions [6,7]. HAp is brittle and weak and the clinical orthopedic and dental applications are limited due to its unfavorable mechanical properties [8,9]. Therefore, it is essential to mechanically support it for the long-term performance. To do that, titanium and its alloys have been used widely as load-bearing implants due to their excellent mechanical toughness, strength, biocompatibility, and corrosion resistance [10–12].

Another approach to enhance mechanical properties of HAp is reinforcing it with other ceramics [13]. To be effective as a reinforcing agent for a ceramic–matrix composite material, the strength of the second phase must be higher than that of the matrix [14]. An appropriate implant material would be a bioceramic composite, formed by a bioactive ceramic such as HAp and a bioinert phase namely zirconia and alumina [15–17]. Zirconia has excellent technological properties and characteristics namely chemical and thermal stability, wear resistance, high strength and fracture toughness, and bioinertness [18–21]. Combining hydroxyapatite and zirconia, favorable mechanical properties and bioactivity is achieved [22,23]. Thus, HAp–zirconia composites have shown promising improvements in strength, hardness, and toughness as compared to the pure HAp [24,25].

The HAp-based composite coatings have been already synthesized via various methods such as sintering [26], micro arc oxidation [27], sol–gel [28,29], mechanosynthesis [30], and simulated body fluid method [31]. In this study, electrophoretic deposition (EPD) and micro arc oxidation (MAO) processes were used to fabricate the HAp–ZrO_2 layers. The phenomenon of electrophoresis has been known since the beginning of the 19th century and it has found applications during the past 40 years mainly

* Corresponding author at: Department of Materials Science and Engineering, North Carolina State University, Raleigh, NC, USA. Tel.: +1 919 917 6962; fax: +1 919 515 7724.
E-mail address: mbayati@ncsu.edu (M.R. Bayati).

0925-8388/$ – see front matter © 2011 Elsevier B.V. All rights reserved.
doi:10.1016/j.jallcom.2011.07.035

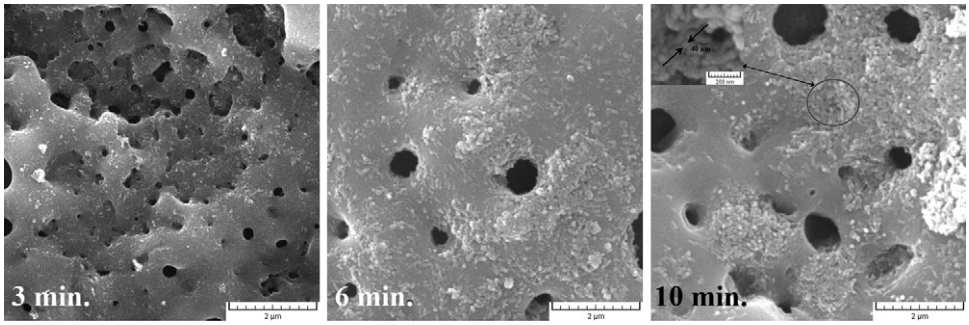

Fig. 1. SEM surface morphology of the composite layers fabricated in the electrolyte A for different times.

in traditional ceramic technology [32,33]. EPD is a simple and inexpensive technique making it possible to synthesize a wide range of coatings with varying morphologies and chemical compositions. This method has been developed to fabricate a variety of dense, nanostructured functional films. Electrophoretic deposition has attracted increasing attention that it can fabricate ceramic films with desirable thickness and parts with complicated shapes. Because of this capability, we employed EPD process to introduce oxide powder to a porous film grown via MAO method. Here, the powder particles dispersed in the liquid medium are attracted and migrate toward the electrode of opposite polarity on which they eventually get deposited [34–37]. MAO is a relatively convenient and effective technique for depositing various functional coatings with porous structures on the surfaces of Ti, Al, Mg and their alloys. In other words, it is a simple and promising approach for fabrication of different categories of oxide layers. It is an electrochemical technique for formation of anodic films by spark/arc microdischarges which move rapidly on the vicinity of the anode surface [38–41]. It is characterized by high productivity, economic efficiency, ecological friendliness, high hardness, good wear resistance, and excellent bonding strength with the substrate [42–44]. Moreover, it is very suitable for modifying various substrates with complex geometries [45]. In biomedical field, MAO has been used to improve the bioactivity of titanium implants [46–49]. More details about MAO [50–54] and EPD [55] methods can be found elsewhere. Employing MAO process, a wide range of ceramic coatings with different chemical compositions can be fabricated [56–62].

In our previous work, ZrO_2–HAp–TiO_2 system was grown onto titanium substrate through EPD-enhanced MAO (EEMAO) process and effect of the applied voltage and the electrolyte concentration on their properties was investigated [63]. In this study, such layers are derived by EEMAO method and the influence of the electrolyte composition and the growth time on physical and chemical features of the layers is investigated. To the best of our knowledge, this is the first time that such layers are fabricated employing EEMAO technique, even though such layers have been already synthesized via other methods with varying morphologies. Beauty of this work is that we could get nano-sized ZrO_2 particles in the layers, while added micron-sized powder to the electrolyte.

2. Experimental

Commercially pure grade II titanium foils with dimensions of 30 mm × 15 mm × 0.5 mm were used as substrate. Before coatings synthesis, the substrates were mechanically polished by abrasive paper No. 600 and, then, chemically etched in diluted HF solution (HF:H_2O = 1:20 vol.%) at room temperature for 30 s. Afterward, the substrates were ultrasonically cleaned in acetone for 15 min. The substrates were washed by distilled water after each step. The electrolytes were prepared by dissolution of the β-glycerophosphate disodium ($C_3H_7Na_2O_6P$, Merck) and calcium acetate ($Ca(CH_3COO)_2$, Panareac) salts with concentrations of 1 and 5 g l^{-1} in 75 vol.% DI-water and 25 vol.% ethanol. Then, micron-sized yttria-stabilized zirconia (8% mol, Tosoh) powder, with concentrations of 1 g l^{-1} (electrolyte A) and 5 g l^{-1} (electrolyte B), was mixed with the suspension by jar-milling for 48 h at room temperature. The pH of the suspensions was adjusted around 11.5 through the addition of sodium phosphate ($Na_3PO_4{\cdot}12H_2O$, Panareac). Reason for choosing such a high pH is inducing negative charge on zirconia particles in the solution. Moreover, HAp and titania can grow easier in the basic electrolytes. Electrolyte temperature was fixed at 70 ± 3 °C employing a water circulating system. The MAO/EPD treatment was carried out in the prepared solutions under the voltage of 350 V (direct current) for various times.

Surface morphology of the layers was examined by scanning electron microscope (TESCAN, Vega II). AFM (Veeco, Auto probe) method was also employed to evaluate surface topography of the fabricated samples. Surface roughness was determined by the AFM original software (Proscan ver. 1.7). X-ray diffraction (Rigaku, Multiflex), energy dispersive X-ray spectroscopy, and X-ray photoelectron spectroscopy (VG Microtech, Twin anode, XR3E2 X-ray source, using Al Kα = 1486.6 eV) techniques were used to study phase structure and chemical composition of the synthesized layers. The peak fitting procedure and interpretation of the XPS results were fulfilled by SDP software ver. 4.1.

3. Results and discussion

SEM surface morphology of the layers grown at different times is depicted in Figs. 1 and 2 where formation of a porous structure is evident. The structural pores from by the electron avalanches taking place on the substrate [59,64]. As is seen, the pores size increases with the treatment time, from about 0.1–0.5 μm for 3 min to about 0.5–1.5 μm for 10 min treatment. It has been shown before that when a structural pore forms by an electrical spark during MAO,

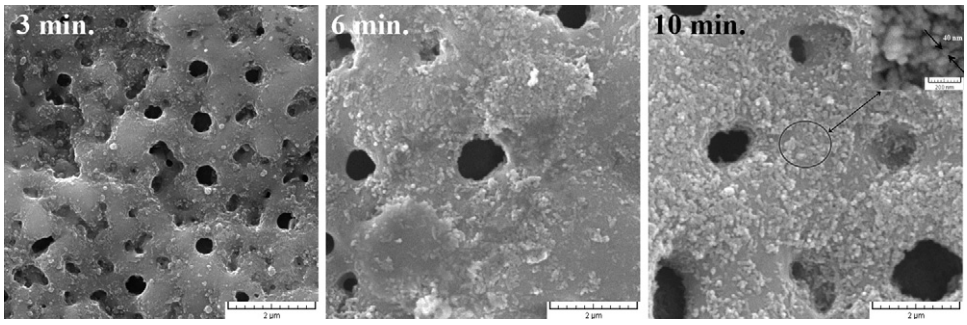

Fig. 2. SEM surface morphology of the composite layers fabricated in the electrolyte B for different times.

it is more susceptible for next electron avalanches. The reason is that these areas have lower breakdown voltages when compared to other areas which are not porous [64]. Sequence of the electrical sparks at one point makes the pores larger. It is worthy to note that these electric sparks are responsible for formation of the structural pores [38]. The utilized micron sized zirconia powder was broken into smaller particles by the electrical spark giving rise to introduction of nano-sized particles to the layers. Obviously, utilizing higher concentrated electrolytes results in formation of larger pores. As the electrolyte electrical resistance, and, consequently, total resistance of the electrochemical cell decrease with increasing the electrolyte concentration, the voltage which is applied on the anode surface increases. Any decrease in circuit resistance results in increasing the current passing through the cell, and, therefore, more energetic electric avalanches take place. Such electric sparks are responsible for formation of larger pores.

It is also clear that the concentration of the zirconia particles on the surface increases with the time and the electrolyte concentration. These particles move toward the anode due to the electrical field between anode and cathode. More zirconia particles are available in the thicker solution, e.g. electrolyte B, resulting in shorter diffusion length in the electrolyte, and for longer deposition time. As a consequence, the zirconia particles can approach and arrive in the anode and the growing layer more easily when the layers are grown in the electrolyte B. Fabricating layers for longer times, the zirconia particles can further accumulate on the vicinity of the anode. Hence, amount of the particles increases with the growth time. It is also observed that nano-sized ZrO_2 particles have formed from the micro-sized powder. Probably, powder dissolved in the electrolytes was broken into finer particles by the electrical sparks.

Another important requirement of HAp coated implants is their adhesion to the body tissues. It is known that as the surface roughness is increased, through mechanical and chemical action, the better osseointegration is achieved [65]. Hence, the surface roughness of the fabricated samples was determined by AFM technique. Fig. 3 shows the surface topography of the layer synthesized for various times in the electrolyte A in a scale of 3 μm × 3 μm. The results depict a rough surface which is usual for MAO-grown layers. The growing layer is locally melted by the electron avalanches (i.e. micro-arcing) taking place on the anode surface. It is anticipated that after the sparks disappeared, the melted zones solidify in the adjacent electrolyte. These successive meltings and solidifications makes the layers roughened. The surface roughness of the layers fabricated for 3, 6, and 10 min was determined as 9.5, 11.6, and 8.1 nm, respectively. Although the surface roughness increases when the time prolongs from 3 to 6 min due to the more meltings and solidifications, another phenomenon is also effective resulting in decreasing the roughness when the layer was treated for 10 min. When the micro arc oxidation is carried out for very long times, the growing layer is sintered resulting in formation a more smooth surface with a lower surface roughness. Since the layers synthesized for 6 min exhibited the highest surface roughness, a better adhesion is anticipated when it is located inside the body.

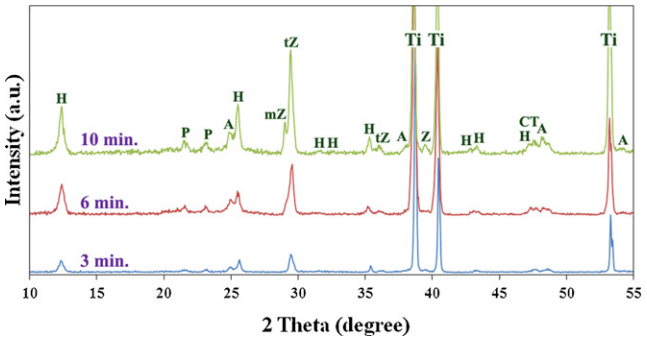

Fig. 4. XRD patterns of the composite layers grown in the electrolyte A for different times (Ti: titanium, A: anatase, H: hydroxyapatite, mZ: monoclinic ZrO_2, tZ: tetragonal ZrO_2, Z: ZrO, CT: $CaTiO_3$, P: α-TCP).

Fig. 4 illustrates the normalized XRD patterns of the composite layers grown for different times in the electrolyte A. Considering the patterns, formation of HAp as well as zirconia with tetragonal and monoclinic structures is confirmed, while fraction of the HAp increases with the growth time. In addition, intensity of the XRD characteristic peaks of the zirconia phases changes depending on the growth time. Because more zirconia particles move toward the anode and accumulate in the vicinity of the layer for longer growth times, the ZrO_2 XRD peaks intensify with the growth time. This conclusion was confirmed by EDX results where the zirconium wt% was determined as 18.1, 29.7, and 41.8% in the layers grown for 3, 6, and 10 min in the electrolyte A, respectively. For longer growth time, the tetragonal ZrO_2 transforms to the monoclinic ZrO_2. It is well known that the anode temperature, during MAO process, increases to several hundred degree centigrade due to the high applied voltages and the electric sparks [38,51]. This phenomenon results in phase transformation of the stabilized zirconia to its monoclinic structure. Tetragonal zirconia is a metastable phase and transforms to the stable monoclinic zirconia at elevated temperature. Such phase transformation, which results in existence of both types of zirconia, has a positive effect on the mechanical properties of the layers. It has been reported that zirconia-based materials exhibit exceptional toughness due to the martensitic transformation of between tetragonal and monoclinic ZrO_2 [66]. Formation of some minor phases is evident. The temperature inside the pores elevates to $\sim 10^4$ K due to the high energy electron avalanches [38,51]. This temperature is high enough to melt the substrate as well as the growing layer. It is anticipated that the molten system dissolves the ZrO_2 particles and other anions to form these minor phases. It should be reminded that negatively charged species are drawn inside the pores and to the molten areas because of the strong electric field between the anode and the cathode which is about 10^6 V m^{-1} [51]. After the electrical spark disappears the molten areas solidify in the adjacent electrolyte.

XRD spectra of the layers grown in the electrolyte B are exhibited in Fig. 5. Phase structure of these layers is to some extent similar

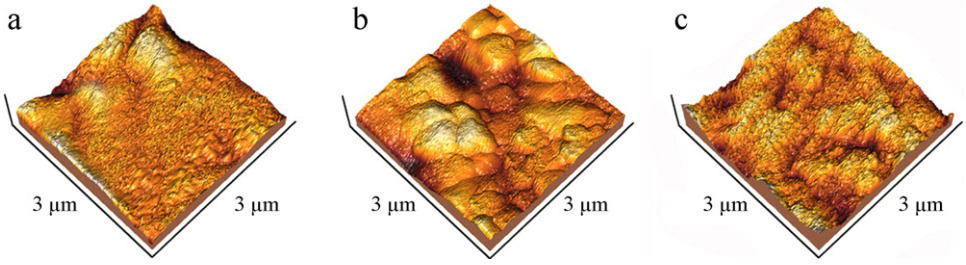

Fig. 3. AFM surface topography of the layers grown in Electrolyte A for: (a) 3, (b) 6, and (c) 10 min.

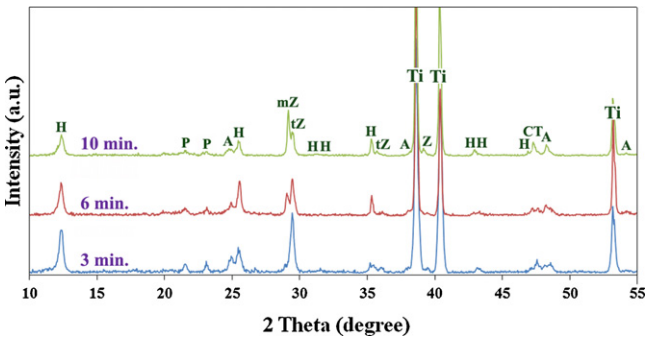

Fig. 5. XRD patterns of the composite layers grown in the electrolyte B for different times (Ti: titanium, A: anatase, H: hydroxyapatite, mZ: monoclinic ZrO_2, tZ: tetragonal ZrO_2, Z: ZrO, CT: $CaTiO_3$, P: α-TCP).

to that of the layers fabricated in the electrolyte A. The most significant difference is that intensity of the XRD peaks of the HAp decreases with the growth time above 6 min. This may be an effect of increasing the electrolyte conductivity with its concentration which results in increasing the current passing the cell and, consequently, the anode temperature. Due to this heat the HAp phase which is stable at the temperatures below 1200 °C [67] decomposes resulting in decreasing the intensity of its characteristic peaks for longer growth times. Besides, this extra heat encourages the tetragonal ZrO_2 to transform to its monoclinic structure. Therefore, this phase transformation takes place faster. The crystalline size of the HAp phase was calculated by the Scherrer equation stating $D = 0.89\lambda/\pi\beta\cos\theta$, where D is the crystal size, λ the X-ray wavelength, β the full width at half maximum of the diffraction peak, and θ is the diffraction angle. The average crystalline size was determined as ~54 nm.

We employed XPS technique in order to investigate surface chemical composition of the composite layers. The results were interpreted according to the C(1s) core level binding energy at 285.0 eV. The XPS investigation was performed on the layer grown in the electrolyte A for 6 min which demonstrated more appropriate phase structure, morphology, and topography. Fig. 6a depicts the Ti($2p_{3/2}$) core level binding energy. The peak fitting was performed with 2 components where the dominant peak (peak B) is assigned to the Ti^{4+} in Ti–O binding. Since the TiO_2 surface loses its oxygen at high temperatures, a small amount of Ti^{3+} (peak A) corresponding to the Ti_2O_3 compound was also detected. The Zr(3d) core level biding energy is shown in Fig. 6b. This peak have 2 components which are attributed to its spin orbit splitting, i.e. Zr($3d_{3/2}$) and Zr($3d_{5/2}$). The peaks A and B are consistent with those of metallic Zr^o($3d_{5/2}$) and Zr^o($3d_{3/2}$), respectively. The peaks C and D, at the binding energies of 180.5 and 181.5 eV, represent existence of Zr^{2+} and formation of ZrO and probably some other non-stoichiometric zirconium oxides (Zr_xO_y). Finally, formation of ZrO_2 compound is confirmed by the peaks E and F located at the binding energies of 182.4 and 183.5 eV. These achievements are in good agreement with those reported by other researchers [68,69]. The P(2p) core level binding energy is exhibited in Fig. 6c which is deconvoluted to the peaks A and B, with binding energies of 132.7 and 134.2 eV. These peaks, which are corresponding to the $2p_{3/2}$ and $2p_{1/2}$ core levels, prove the existence of phosphor in HAp structure. The O(1s) core level biding energy is depicted in Fig. 6d which can be deconvoluted to 5 distinct peaks representing that there are 5 different O-bindings in the layers. The peak A, located at the binding energy of 529.8 eV, is assigned to the oxygen in the oxides lattice namely ZrO_2 and TiO_2. The peak B, at the binding energy of 530.7 eV, corresponds to the oxygen in nonstoichiometric zirconium oxides. The peak C at the binding energy of 531.85 eV represents the –OH groups in the HAp molecules. In addition, oxide free surfaces are always hydrated in the atmosphere. Therefore, the chemisorbed hydroxyl groups are always seen in the XPS patterns obtained from the oxide films. The peaks C and D, located at the biding energies of 533.1 and 534.4 eV, reveal existence of oxygen as O^- and H_2O with descending binding

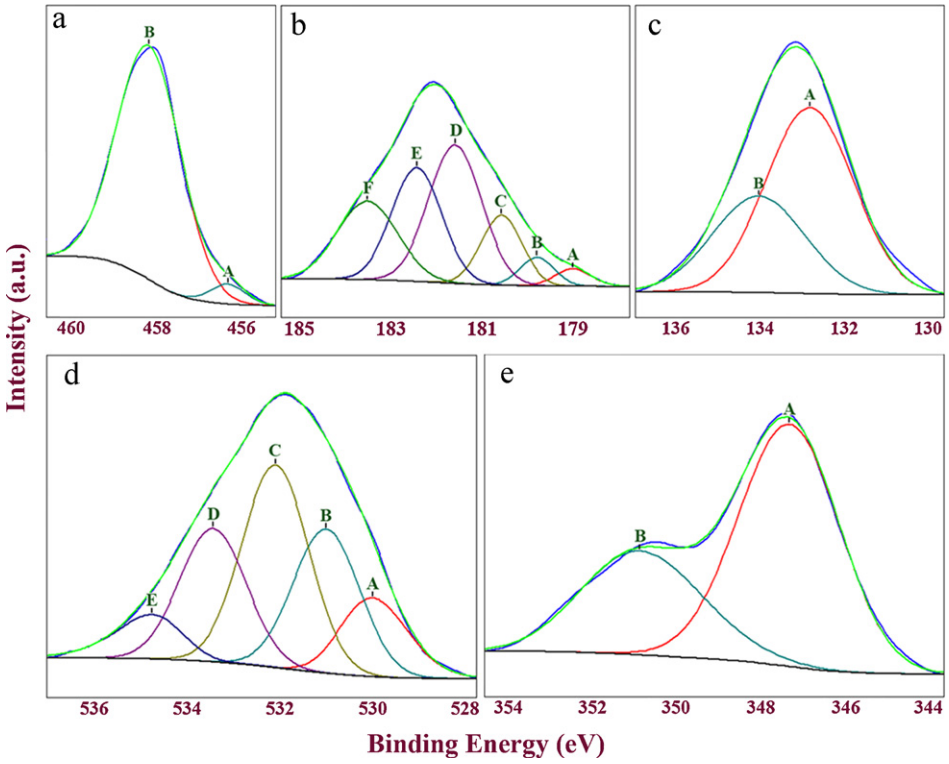

Fig. 6. XPS core level binding energies in the layers grown in the electrolyte A for 6 min (referenced to the C(1s) at 285.0 eV).

energy, respectively. Since the layers were porous and fabricated in aqueous solutions, water may be trapped in the pores. Meanwhile, the layers were enshrouded by an oxygen plasma during the MAO treatment. This phenomenon can be the cause of attaching oxygen radicals to the surface. Finally, Fig. 6e shows the XPS spectra of Ca(2p) core level binding energy. The peaks A and B, with binding energies of 347.7 and 351.2 eV, are attributed to the spin–orbit splitting of the Ca(2p) components, namely $Ca(2p_{3/2})$ and $Ca(2p_{1/2})$. They are consistent with those of calcium in the HAp structure. Small deviations in the binding energies of P(2p) and Ca(2p) core levels are due to the formation of the minor phases introduced earlier.

A plausible mechanism for formation of HAp–ZrO_2–TiO_2 composite layers via EEMAO method was proposed in our previous work [63]. When ZrO_2 particles are dispersed in a basic solution, they are negatively charged, as elucidated earlier. In the meantime, structural pores form as a result of the electric sparks. The ZrO_2 particles are drawn toward the anode by the electric field between the poles of the electrochemical cell. When they arrive in the regions close to the anode, they are sublimated in the discharge areas and drawn into the gas layer, i.e. oxygen layer, enshrouding the substrate. Afterward, they are accelerated by the potential difference in the gas layer and implanted in the growing layer. Since ZrO_2 phase was detected by both XRD and XPS techniques, it can be concluded that they have formed not only on the surface, but also in the layers depth because of the so-called acceleration and implantation phenomena.

4. Conclusions

Fabrication of ZrO_2–HAp–TiO_2 nanostructured porous layers via MAO/EPD hybrid technique was reported. The layers had porous morphology and a rough surface where the pores size and the surface roughness increased with the time and the electrolyte concentration. Anatase, hydroxyapatite, monoclinic ZrO_2, and tetragonal ZrO_2 were the main phases of the layers. The nanosized zirconia particles (d = 20–60 nm) were loaded on the surface and in the layers depth.

Acknowledgements

The authors would like to express their sincere appreciations to all personnel working in the Ceramics Synthesis Laboratory at Iran University of Science and Technology. Meanwhile, financial support of Iran National Science Foundation (INSF) is highly appreciated.

References

[1] L.L. Hench, J. Am. Ceram. Soc. 74 (1991) 1487.
[2] W. Suchanek, M. Yoshimura, J. Mater. Res. 13 (1998) 796.
[3] I. Mobasherpour, M. Soulati Heshajin, A. Kazemzadeh, M. Zakeri, J. Alloys Compd. 430 (2007) 330.
[4] M.M. Hukovic, E. Tkalcec, A. Kwokal, J. Piljac, Surf. Coat. Technol. 165 (2003) 40.
[5] E. Banks, S. Nakajima, L.C. Shapiro, O. Tilevitz, J.R. Alonzo, R.R. Chianelli, Science 198 (1977) 1164.
[6] I.R. Gibson, S.M. Best, W. Bonfield, J. Am. Ceram. Soc. 85 (2002) 2771.
[7] J.M. Gomez-Vega, E. Saiz, A.P. Tomsia, T. Oku, K. Suganuma, G.W. Marshall, et al., Adv. Mater. 12 (2000) 894.
[8] W.R. Rao, R.F. Boehm, J. Dent. Res. 53 (1974) 1351.
[9] G. De With, H.J.A. Van Dijck, N. Hattu, K. Prijs, J. Mater. Sci. 16 (1981) 1592.
[10] X.Y. Liu, K.C. Paul, C.X. Ding, Mater. Sci. Eng. R 47 (2004) 49.
[11] J. Kunze, L. Muller, J.M. Macak, P. Greil, P. Schmuki, F.A. Muller, Electrochim. Acta 53 (2008) 6995.
[12] D.O. Flamini, S.B. Saidman, Electrochim. Acta 55 (2010) 3727.
[13] P. Ducheyne, M. Marcolongo, E. Schepers, in: L.L. Hench, J. Wilson (Eds.), An Introduction to Bioceramic, World Scientific Publishing Co., Singapore, 1993, p. 281.
[14] Y.M. Kong, S. Kim, H.E. Kim, J. Am. Ceram. Soc. 82 (1999) 2963.
[15] B. Basu, B.K. Sarkar, J. Mater. Res. 11 (1996) 3057.
[16] B. Basu, J. Vleugels, O. Van Der Biest, J. Alloys Compd. 365 (2004) 266.
[17] R. Stevens, Trans. Brit. Ceram. Soc. 80 (1981) 81.
[18] F.C. Jentoft, A. Fischer, G. Weinberg, U. Wild, R. Schlgl, Stud. Surf. Sci. Catal. 130 (2000) 209.
[19] C.L. Hyun, L. Doohwan, Y.L. Ok, K. Soonho, T.K. Yong, K. Eun-Yong, D.P. Eun, Stud. Surf. Sci. Catal. 167 (2007) 201.
[20] K. Tsukuma, K. Ueda, M. Shimada, J. Am. Ceram. Soc. 68 (1985), c-4–c-5.
[21] O.N. Grigoryev, S.A. Firstov, O.A. Babiy, G.E. Homenko, J. Mater. Sci. 29 (1994) 4633.
[22] M. Ferraris, H.E. Verne, P. Appendino, C. Moisescu, A. Krajewski, A. Ravaglioli, Biomaterials 21 (2000) 765.
[23] M. Bosetti, E. Verne, M. Ferraris, A. Ravaglioli, M. Cannas, Biomaterials 22 (2001) 987.
[24] J.M. Wu, T.S. Yeh, J. Mater. Sci. 23 (1988) 3771.
[25] K.A. Khalil, S.W. Kim, H.Y. Kim, Mater. Sci. Eng. A 456 (2007) 372.
[26] J. Li, H. Liao, L. Hermansson, Biomaterials 17 (1996) 1787.
[27] K. Nan, T. Wu, J. Chen, S. Jiang, Y. Huang, G. Pei, Mater. Sci. Eng. C 29 (2009) 1554.
[28] J.X. Zhang, R.F. Guan, X.P. Zhang, J. Alloys Compd. 509 (2011) 4643.
[29] M. Mazrooei Sebdani, M.H. Fathi, J. Alloys Compd. 509 (2011) 2273.
[30] C. Mochales, J. Alloys Compd. (2011).
[31] M. Zheng, D. Fan, X. Li, J. Zhang, Q. Liu, J. Alloys Compd. 489 (2010) 211.
[32] A.R. Boccaccini, I. Zhitomirsky, Curr. Opin. Solid State Mater. Sci. 6 (2002) 251.
[33] W.E. Windes, J. Zimmerman, I.E. Reimanis, Surf. Coat. Technol. 157 (2002) 267.
[34] L. Miao, S. Cai, Z. Xiao, J. Alloys Compd. 490 (2010) 422.
[35] A.G. Bhosale, R. Joshi, K.M. Subhedar, R. Mishra, S.H. Pawar, J. Alloys Compd. 503 (2010) 266.
[36] R. Ma, I. Zhitomirsky, J. Alloys Compd. 509S (2011) S510.
[37] J. Chen, H. Fan, X. Chen, P. Fang, C. Yang, S. Qiu, J. Alloys Compd. 471 (2009) L51.
[38] A.L. Yerokhin, X. Nie, A. Leyland, A. Matthews, S.J. Dowey, Surf. Coat. Technol. 122 (1999) 73.
[39] A.L. Yerokhin, A. Leyland, A. Matthews, Surf. Coat. Technol. 200 (2002) 172.
[40] X. Sun, Z. Jiang, S. Xin, Z. Yao, Thin Solid Films 471 (2005) 194.
[41] P. Gupta, G. Tenhundfeld, E.O. Daigle, D. Ryabkov, Surf. Coat. Technol. 201 (2007) 8746.
[42] A.L. Yerokhin, X. Nie, A. Leyland, A. Matthews, Surf. Coat. Technol. 130 (2000) 195.
[43] W. Xue, C. Wang, R. Chen, Z. Deng, Mater. Lett. 52 (2002) 435.
[44] W. Xue, Z. Deng, R. Chen, T. Zhang, Thin Solid Films 372 (2000) 114.
[45] D. Wei, Y. Zhou, D. Jia, Y. Wang, Acta Biomater. 3 (2007) 817.
[46] H. Ishizawa, M. Ogino, J. Biomed, Mater. Res. 29 (1995) 65.
[47] X.L. Zhu, K.H. Kim, Y.S. Jeong, Biomaterials 22 (2001) 2199.
[48] Y. Han, S.H. Hong, K. Xu, Surf. Coat. Technol. 168 (2003) 249.
[49] W.H. Song, Y.K. Jun, Y. Han, S.H. Hong, Biomaterials 25 (2004) 3341.
[50] J.M. Wheeler, C.A. Collier, J.M. Paillard, J.A. Curran, Surf. Coat. Technol. 204 (2010) 3399.
[51] A.L. Yerokhin, V.V. Lyubimov, R.V. Ashitkof, Ceram. Int. 24 (1998) 1.
[52] M.R. Bayati, A.Z. Moshfegh, F. Golestani-Fard, Electrochim. Acta 55 (2010) 3093.
[53] M.R. Bayati, A.Z. Moshfegh, F. Golestani-Fard, Electrochim. Acta 55 (2010) 2760.
[54] M.R. Bayati, R. Molaei, A. Kajbafvala, S. Zanganeh, H.R. Zargar, K. Janghorban, Electrochim. Acta 55 (2010) 5786.
[55] M. Ammam, J. Fransaer, Electrochim. Acta 55 (2010) 3206.
[56] M.R. Bayati, F. Golestani-Fard, A.Z. Moshfegh, Appl. Catal. A: Gen. 382 (2010) 322.
[57] M.R. Bayati, A.Z. Moshfegh, F. Golestani-Fard, R. Molaei, Mater. Chem. Phys. 124 (2010) 203.
[58] M.R. Bayati, A.Z. Moshfegh, F. Golestani-Fard, Appl. Surf. Sci. 256 (2010) 2903.
[59] M.R. Bayati, F. Golestani-Fard, A.Z. Moshfegh, Mater. Chem. Phys. 120 (2010) 582.
[60] M.R. Bayati, H. Zargar, R. Molaei, F. Golestani-Fard, E. Kajbafvala, S. Zanganeh, Colloids Surf. A 355 (2010) 187.
[61] M.R. Bayati, A.Z. Moshfegh, F. Golestani-Fard, Appl. Catal. A: Gen. 389 (2010) 60.
[62] M.R. Bayati, A.Z. Moshfegh, F. Golestani-Fard, Mater. Lett. 64 (2010) 2215.
[63] F. Samanipour, M.R. Bayati, F. Golestani-Fard, H.R. Zargar, T. Troczynski, A.R. Mirhabibi, Colloid Surf. B: Biointerface 86 (2011) 14.
[64] M.R. Bayati, F. Golestani-Fard, A.Z. Moshfegh, Appl. Surf. Sci. 256 (2010) 4253.
[65] S. Hirakura, T. Kobayashi, S. Ono, Y. Oaki, H. Imai, Colloids Surf. B 79 (2010) 131.
[66] A. Rapacz-Kmita, A. Slosarczyk, Z. Paszkiewicz, J. Eur. Ceram. Soc. 26 (2006) 1481.
[67] O. Albayrak, O. El-Atwani, S. Altintas, Surf. Coat. Technol. 202 (2008) 2482.
[68] J. Park, J.K. Heo, Y.C. Kang, Bull. Korean Chem. Soc. 31 (2010) 397.
[69] S. Wang, C. Liu, F. Shan, Acta Metall. Sin. (Engl. Lett.) 22 (2009) 161.